Ambient-Dried, 3D-Printable and Electrically Conducting Cellulose Nanofiber Aerogels by Inclusion of Functional Polymers

ADVANCED FUNCTIONAL MATERIALS
www.afm-journal.de

Ambient-Dried, 3D-Printable and Electrically Conducting Cellulose Nanofiber Aerogels by Inclusion of Functional Polymers

Hugo Françon, Zhen Wang, Andrew Marais, Katarzyna Mystek, Andrew Piper, Hjalmar Granberg, Abdellah Malti, Paul Gatenholm, Per A. Larsson, and Lars Wågberg**

This study presents a novel, green, and efficient way of preparing crosslinked aerogels from cellulose nanofibers (CNFs) and alginate using non-covalent chemistry. This new process can ultimately facilitate the fast, continuous, and large-scale production of porous, light-weight materials as it does not require freeze-drying, supercritical CO_2 drying, or any environmentally harmful crosslinking chemistries. The reported preparation procedure relies solely on the successive freezing, solvent-exchange, and ambient drying of composite CNF-alginate gels. The presented findings suggest that a highly-porous structure can be preserved throughout the process by simply controlling the ionic strength of the gel. Aerogels with tunable densities (23–38 kg m^{-3}) and compressive moduli (97–275 kPa) can be prepared by using different CNF concentrations. These low-density networks have a unique combination of formability (using molding or 3D-printing) and wet-stability (when ion exchanged to calcium ions). To demonstrate their use in advanced wet applications, the printed aerogels are functionalized with very high loadings of conducting poly(3,4-ethylenedioxythiophene):tosylate (PEDOT:TOS) polymer by using a novel in situ polymerization approach. In-depth material characterization reveals that these aerogels have the potential to be used in not only energy storage applications (specific capacitance of 78 F g^{-1}), but also as mechanical-strain and humidity sensors.

1. Introduction

Aerogels are synthetic materials exhibiting exceptional properties such as ultra-low density and thermal conductivity.[1–3] Despite numerous attempts at defining this material, a certain confusion regarding the semantics still prevails. According to the IUPAC terminology, aerogels are a subset of gels comprising a microporous solid in which the disperse phase is gaseous.[4] However, aerogels are also often defined according to their fabrication protocol, i.e., as porous materials derived from gels where the liquid phase is replaced by a gas.[5] Owing to their low solid content and small average pore size,[6] aerogels have historically been developed as thermal insulators.[7] They have also shown promise in water purification systems, energy storing/harvesting devices, oil absorbents and acoustic insulators.[8–14] Nonetheless, due to the complex processes required to prepare aerogels, their preparation on an industrial scale has yet to be realized. Numerous sol-gel methods have been reported to produce gels of different structures and properties.[5] These gels are either frozen and then freeze-dried or dried by critical-point drying.[15] These two processes are difficult to implement at an industrial scale as they are costly, time and energy consuming, and require batch processing.[16] Silica-based aerogels are an example of commercially successful aerogels,[17] although suffering from their inherent brittleness, lack of formability, and high processing cost.[18,19] To mitigate these issues, aerogels made from numerous other starting materials have been suggested.[20,21]

Cellulose is an abundant linear biopolymer of glucose units which, in nature, is assembled in highly ordered, long, and thin nanostructures called cellulose nanofibers (CNFs). CNFs are known for their low thermal expansion coefficient and their high stiffness, with an elastic modulus of 138 GPa.[22,23] When extracted from delignified wood fibers, they typically have a width of 4 nm and a length of 500–2000 nm; dependent on choice of raw material and how it was processed.[24] As the CNFs are tightly packed in the fiber wall lamellae, their isolation requires costly and high-energy mechanical treatments. The cost of the extraction process can, however, be

H. Françon, Dr. Z. Wang, Dr. A. Marais, K. Mystek, Dr. A. Piper, Dr. A. Malti, Dr. P. A. Larsson, Prof. L. Wågberg
Department of Fibre and Polymer Technology
KTH Royal Institute of Technology
Teknikringen 58, SE-100 44 Stockholm, Sweden
E-mail: francon@kth.se; wagberg@kth.se

Dr. H. Granberg
RISE Innventia AB
Papermaking and Packaging
Box 5604, SE-114 86 Stockholm, Sweden

Prof. P. Gatenholm
Department of Chemistry and Chemical Engineering
Chalmers University of Technology
Kemigården 4, SE-412 69 Gothenburg, Sweden

The ORCID identification number(s) for the author(s) of this article can be found under https://doi.org/10.1002/adfm.201909383.

DOI: 10.1002/adfm.201909383

significantly reduced by the introduction of charged moieties in the cellulose backbone. These charges lead to electrostatic repulsion between neighboring CNFs, thus counteracting the strong inter-fibrillar interactions holding the fiber wall together and facilitating an efficient extraction of individualized CNFs. In this respect, TEMPO oxidation and carboxymethylation are two of the most commonly used chemical pathways to introduce carboxyl groups in cellulose.[25–28]

Studies of the colloidal stability of carboxymethylated CNFs have reported the formation of gels at low solid contents,[29,30] that can be freeze-dried into aerogels. These nanocellulose aerogels are highly porous, light, and soft materials.[31,32] Benefiting from the structure and properties of the CNFs, these aerogels possess high specific surface areas and readily absorb most liquids.[32–34] Moreover, CNF aerogels are easy to tailor using classical cellulose chemistry or the layer-by-layer approach.[32,35]

Freeze-dried CNF aerogels owe their physical integrity to a fairly small area of inter-fibrillar contact and disintegrate when placed in water. However, aerogels need to be wet-stable to be used in advanced wet applications, such as bioelectronics. This is commonly achieved by crosslinking the fibrillar structure, either in the dry or the wet state, with covalent inter-fibrillar bonds such as ether, urethane, ester, or hemiacetal linkages.[35–38] Recent studies demonstrated the preparation of wet-stable aerogels from dialdehyde CNFs by using a simple freezing, thawing, and solvent exchange procedure.[39–41] Thanks to the absence of critical point drying and freeze-drying, this process could presumably be fairly easily made continuous and meet industrial requirements both in terms of energy consumption and production rate. However, this preparation procedure requires sodium metaperiodate, whose efficient handling and recovery is still economically and practically challenging.[42,43]

Algal polysaccharides have recently shown great promise in the preparation of wet-stable cellulosic networks.[44,45] Due to their chemical similarity, algal polysaccharides and CNFs can assemble into double networks.[46] Known for their ability to form supramolecular assemblies when coordinated with multivalent ions, these natural polysaccharides can, therefore, be used to lock CNF networks and make them wet stable. A typical example of such gelling polysaccharides is alginate, commonly extracted from brown algae. This linear copolymer of guluronic acid and mannuronic acid is known to form stable intermolecular crosslinked regions when complexed with divalent counterions.[47] The supramolecular organization of alginate is described by the commonly accepted, but sometimes challenged,[48] "egg-box" model.[49]

Aerogels have both interconnected porous structures and high specific surface areas. Therefore, they could be used as substrates to prepare devices with high loadings of active materials. When functionalizing cellulose aerogels it is essential to have a good interaction between the cellulose and the added components. In this respect, CNFs have been shown to be highly compatible with numerous conducting and redox-active polymers.[36,39,50,51] Among the commercially available conducting polymers, poly(3,4-ethylenedioxythiophene) (PEDOT) distinguishes itself by displaying high conductivity, good biocompatibility, and low toxicity.[52] PEDOT and CNFs have been combined to prepare a variety of organic electronic devices; an exemplary work of this was published by Malti et al. in which the PEDOT-CNF composite displayed unprecedented high conductivity of both ions and electrons.[53,54] Recent studies also show that PEDOT can self-assemble into interconnected, highly-conducting structures along CNFs.[55,56]

This study presents a novel and environment friendly method to prepare wet-stable organic aerogels. Gels of carboxymethylated CNFs and alginate were prepared at different ionic strengths and with countercations of different valencies. These gels were turned into highly porous substrates by freezing, thawing, solvent-exchange, and finally ambient drying. Wet stability was achieved after post-treating the aerogels in solutions containing multivalent ions. Advanced applications often require complex material shaping and design. Therefore, the possibility of 3D printing the CNF-alginate double networks has been demonstrated and organic aerogels of intricate shapes were prepared. It was also shown that highly conductive aerogels with very high loadings of PEDOT could be prepared using an in situ polymerization approach. These functionalized aerogels were then characterized as energy storage as well as pressure and humidity sensor materials.

2. Aerogels from Cellulose Nanofibers and Sodium Alginate

2.1. Principles of Aerogel Making

Aerogels were prepared according to the processing route shown in **Figure 1**a (see Experimental Section for a complete description of the procedure). Two different carboxymethylated CNF-to-alginate ratios were studied in detail (80:20 w/w and 100:0 w/w), as well as three different ionic strengths of sodium chloride and calcium chloride (no added salt, 10×10^{-3} M and 100×10^{-3} M ionic strength additions).

The formation of a porous structure that withstands ambient drying relies on the ice-templating of colloidal systems.[57] As the water in the gel freezes, the CNFs are gradually excluded from the growing ice crystals. The distance between CNFs consequently decreases, forcing them together into an interconnected lamellar structure. By using suitable gel formulations, the lamellae can be made strong enough to withstand thawing of the ice and ambient drying from a low-boiling-point, non-polar solvent such as acetone. As shown in Figure 1b,c, the formation of a stable, porous structure largely depends on the ionic strength within the gel during mixing and freezing. Without any salt added, the CNF networks collapsed during drying. However, the aerogels prepared at higher ionic strengths, both in presence of NaCl and $CaCl_2$ (10×10^{-3} M and 100×10^{-3} M ionic strength), underwent significantly lower shrinkage upon drying, thus displaying lower densities. CNFs and charged polysaccharides such as alginate have been shown to form strong networks in the presence of multivalent, complexing cations such as Ca^{2+}.[46] However, none of the aerogels made by adding 100×10^{-3} M of monovalent NaCl collapsed significantly during drying, indicating that the strength of the porous structure cannot solely be explained by

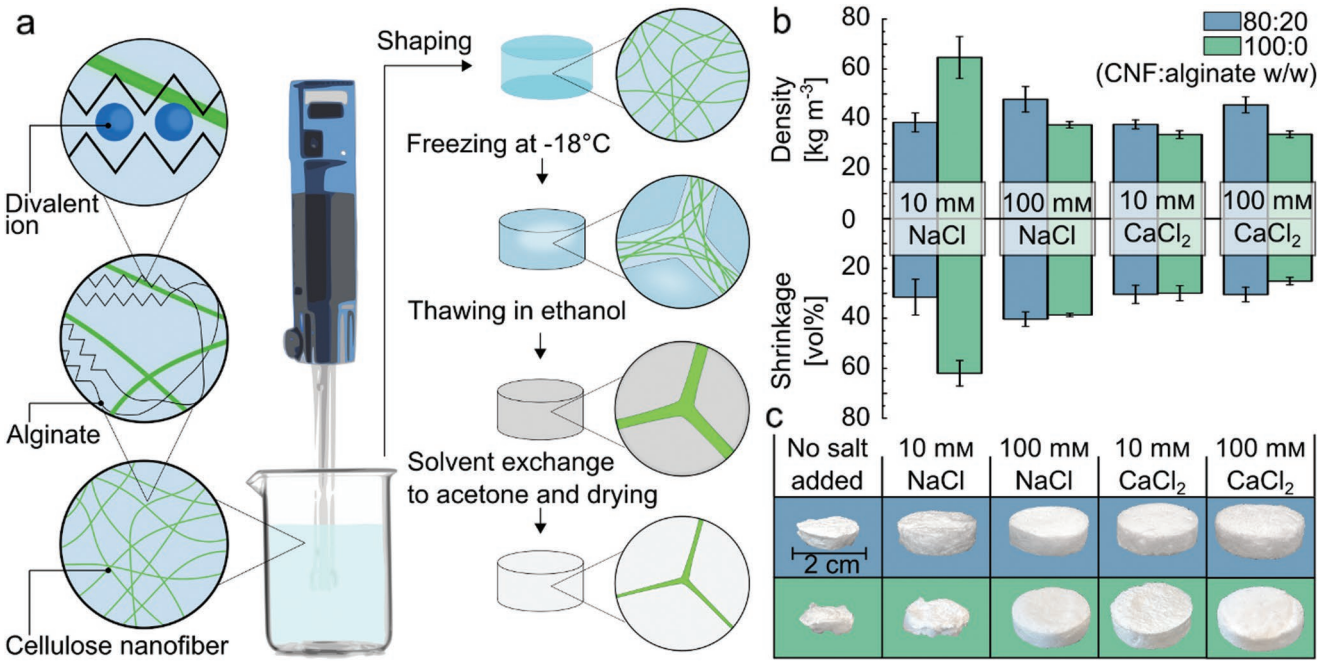

Figure 1. a) Schematic summary of the protocol for preparing the aerogels using CNFs, alginate, and salt. b) Densities, volumetric shrinkages, and c) photographs of aerogels prepared from mixtures of different ionic strengths, alginate, and CNF contents (all photographs are presented at the same scale).

this complexation mechanism. A look at the colloidal stability of the system provides an insight into the phenomena taking place. Both carboxymethylated CNFs and alginate carry a significant amount of carboxylic groups. At pHs close to neutral, which corresponds to the conditions used for the preparation of the aerogels, these functional groups are deprotonated, thus negatively charged. When this highly-charged colloidal system is frozen at low ionic strengths, electrostatic repulsion between the nanofibers inhibits physical contact. As salt is added to the system, repulsive electrostatic forces are screened over a longer range, and the distance at which the nanofibers start repelling each other decreases.[29] Therefore, a closer contact between the nanofibers, resulting in mechanically stronger lamellae, is expected when freezing the gels prepared with additions of either NaCl or CaCl. Consequently, these samples could resist the structural stress caused by the destructive capillary forces during evaporation; whereas the ones prepared without any salt addition largely collapsed. It is worth noting that ice crystals have been shown to push CNFs close enough toward each other to establish chemical contact in a previous study.[41]

As shown in Figure 1b,c, the presence of 20 wt% alginate only seems to have a significant impact on the volumetric shrinkage and density of the aerogels prepared with 10×10^{-3} M NaCl. The samples prepared without any alginate in 10×10^{-3} M NaCl were largely deformed or collapsed, whereas those prepared with 20 wt% alginate and 10×10^{-3} M NaCl retained their highly porous structure throughout the drying. This positive effect of adding alginate could be explained by a reinforcement of the lamellar structure owing to the entanglement of the alginate molecules with the CNFs, and/or by better electrostatic screening of their charges. Bearing a significantly higher charge than the CNFs, alginate brings a large amount of counter ions into the system and thus causes a significant increase of the ionic strength in the lamella during freezing. Samples prepared with the addition of 10×10^{-3} M $CaCl_2$ present similar densities and volumetric shrinkages, regardless whether alginate was added to the formulation or not. This observation indicates that CNFs form stronger structures using $CaCl_2$ than NaCl, which is in accordance with previously reported studies.[58] For the sake of clarity, the aerogels will, from now on, be named according to following notation: "x:y z $\times 10^{-3}$ M S", where x corresponds to the weight fraction of CNFs, y the weight fraction of alginate, z the added ionic strength, and S is the type of salt added; NaCl or $CaCl_2$.

2.2. Achieving Wet-Stability

Wet-stability (the ability of a material to keep its structural integrity when handled in the wet-state) is a property that cellulose aerogels must possess to be used in numerous advanced applications, such as in energy storage devices with liquid electrolytes. In this study, the wet-stability of the materials was assessed as their ability to endure four consecutive compression cycles of increasing maximum compressive strain (20%, 40%, 60%, and 80%) in the wet state. Prior to compression testing, the samples were soaked overnight, from the dry state, in different salt solutions.

None of the samples discussed in Section 2.1 endured the cyclic testing after being soaked in an NaCl solution. A representative sample is shown in **Figure 2**a, where an 80:20 10×10^{-3} M $CaCl_2$ sample was soaked in a 1 M NaCl solution prior to testing, and broke at a compressive strain of about 40%. However, the same sample became wet-stable when soaked in

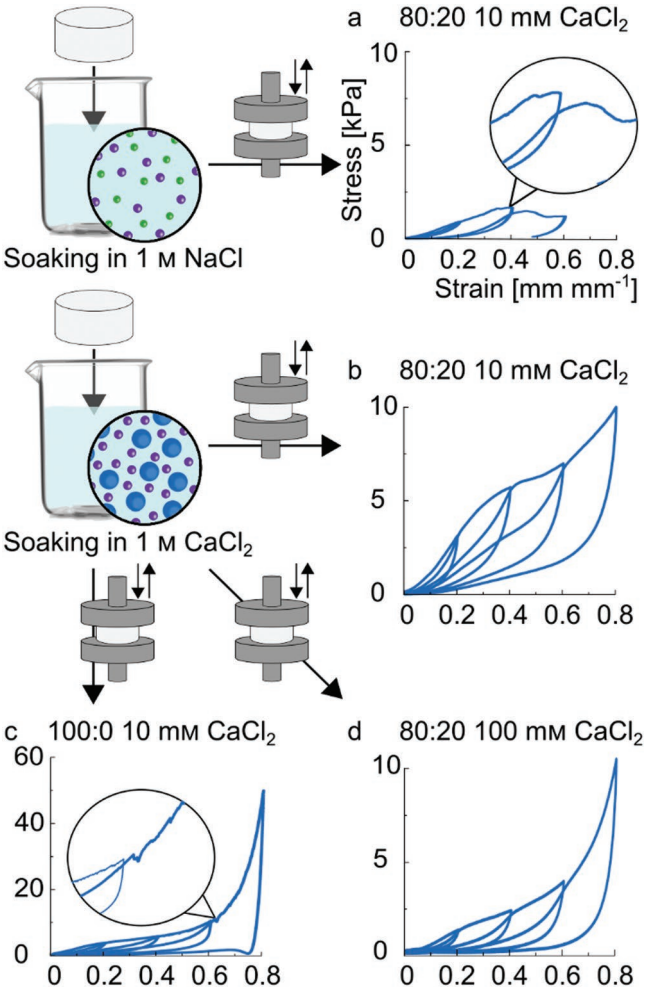

Figure 2. Assessing the wet stability of the aerogels by soaking them in different salt solutions from the dry state and submitting them to compression cycles with increasing maximum strains (sample compositions abbreviated as "x:y z × 10^{-3} M S" where *x* corresponds to the weight fraction of CNFs, *y* the weight fraction of alginate, *z* the added ionic strength, and *S* is the type of salt added during aerogel making; NaCl or $CaCl_2$). The plots show that only the samples containing alginate and soaked in 1 M $CaCl_2$ (b and d) endured the four consecutive compression cycles without noticeable structural damage and, consequently, were deemed "wet-stable."

1 M $CaCl_2$, as it could successfully be deformed to 80% compression without any noticeable structural damage (Figure 2b). To investigate the reasons for the material's wet-stability, 100:0 10 × 10^{-3} M $CaCl_2$ samples were also soaked in a 1 M $CaCl_2$ solution and compressed. As shown in Figure 2c, these alginate free samples started to mechanically fail at compression strains of about 60%. In summary, only samples containing alginate and that have undergone an ion-exchange in $CaCl_2$ solution displayed complete wet-stability.

In a previous study, CNF-alginate nanocomposites with high wet-strengths were prepared by soaking dry nanocomposite films in $CaCl_2$ solutions.[46] The Young's moduli, tensile strengths, and toughnesses of these films were far superior to those of pure CNFs or pure alginate. However, when a wet CNF-alginate film was soaked in a calcium solution, i.e., without any intermediate drying, no strengthening was observed. The authors described the structure of the material as two distinct, interpenetrated networks of CNFs and alginate which are, in the dry state, close enough to for the calcium ions to induce a significant attractive interaction between their different components. The structure of these nanocomposite films is similar to that of the lamellae formed in the ice-templated aerogels described in this work. A similar reinforcement mechanism can hence be also presumed in these wet-stable aerogels.

Aerogels prepared from gels of higher ionic strengths also showed wet-stability, but were significantly weaker in the wet state (Figure 2d). In a previous study, CNFs were shown to severely aggregate when the ionic strength addition was increased from 10 to 100 × 10^{-3} M.[29] Hypothetically, when forced together by growing ice crystals, aggregates would form lamellar structures that are more loosely bound than the ones formed from individual CNFs. Therefore, the lamellae formed at 100 × 10^{-3} M ionic strength addition should expectedly be mechanically weaker than those formed at 10 × 10^{-3} M. The wet mechanical properties of the resulting aerogels are then expected to be worse when the starting ionic strength addition increases from 10 to 100 × 10^{-3} M. Consequently, the aerogels presented in the latter parts of this study were prepared using 10 × 10^{-3} M $CaCl_2$, as they display both low density and good mechanical properties in the wet-state. Although the aerogels were soaked overnight as a standard procedure, they displayed wet-stability as soon as they were fully hydrated with calcium solutions (with ionic strength in the 0.1–1 M range). Consequently, the kinetics of the ion exchange to calcium were not further investigated.

2.3. Tailoring Structural and Mechanical Properties of Aerogels

As shown in **Figure 3**a, the prepared aerogels display an open and porous structure with pore radii ranging from a few tens to a few hundreds of micrometers. The structure is made of cell windows, which meet three by three into struts (Figure 3b). Similar structures and pore sizes have been reported for low density materials prepared by freezing CNFs.[31,32,39,59] Figure 3a also shows that the microstructure seems unaffected by the ionic strength of $CaCl_2$ used during material preparation. This observation is supported by automated porosimetry measurements (Figure 3c),[60] as the cumulative pore volume distributions of the materials prepared with additions of 10 × 10^{-3} M and 100 × 10^{-3} M $CaCl_2$ both show average pore diameters of about 60 µm. This indicates that the size of the ice crystals formed during freezing is not significantly altered over the range of salt concentrations tested.

Although the autoporosimeter cannot probe pore diameters below 4 µm, it is possible to determine the volume of water left in smaller pores by weighing the samples before and after the measurement. Aerogels prepared with additions of 10 × 10^{-3} M $CaCl_2$ and 100 × 10^{-3} M $CaCl_2$ were thereby found to retain 35% and 21% (v/v) of the initially absorbed water in pores with diameters below 4 µm, respectively. When water is frozen at −18 °C from ambient temperature, it is highly unlikely to form ice crystals and, consequently, pores in an ice-template structure that are smaller than 4 µm.[61] A significant

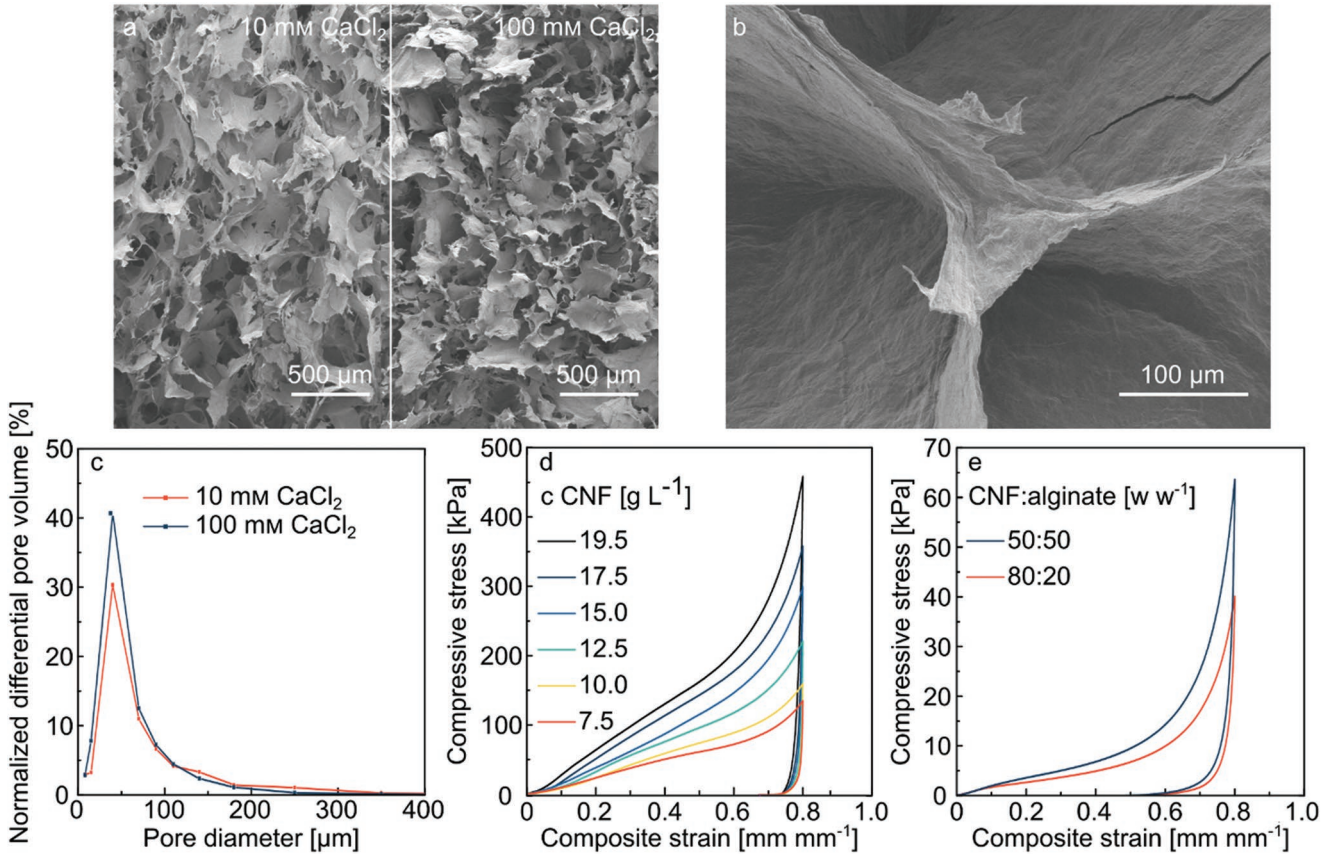

Figure 3. a) Scanning electron microscope (SEM) micrographs of 80:20 aerogels prepared with additions of 10×10^{-3} M $CaCl_2$ (left) and 100×10^{-3} mM $CaCl_2$ (right), b) SEM micrograph of the windows and struts of an 80:20 10×10^{-3} M $CaCl_2$ aerogel. c) Normalized differential pore volume distributions of 80:20 10×10^{-3} M $CaCl_2$ and 80:20 100×10^{-3} M $CaCl_2$ aerogels. d) Compression curves of 80:20 10×10^{-3} M $CaCl_2$ aerogels in the dry state prepared from different initial CNF concentrations. e) Compression curves of 80:20 10×10^{-3} M $CaCl_2$ and 50:50 10×10^{-3} M $CaCl_2$ aerogels in the wet state.

amount of the absorbed water is hence present inside the windows and struts, which are constituted of a nanostructured CNF and alginate double network. Consequently, the structure of the wet aerogel presents a bimodal pore size distribution, with both pores on the 10s of micrometer scale and on the nanometer scale. These aerogels are particularly interesting for liquid absorbency applications, as larger pores enable a fast spreading and smaller pores retain liquids at high pressures.[62]

Aerogels prepared with 10×10^{-3} M $CaCl_2$ retained more water in pores with diameters below 4 µm than for the ones prepared with 100×10^{-3} M $CaCl_2$ (with corresponding volume fractions of 35% and 21%, respectively). This indicates that a greater fraction of the total aerogel volume corresponds to the nanopores in the samples prepared at lower salt concentrations. As discussed in the previous section, a greater ionic strength could potentially lead to increased aggregation of the CNFs. Hence, the struts and windows of the aerogels prepared at 100×10^{-3} M $CaCl_2$ are expected to be made of a more aggregated, therefore less porous, CNF-alginate double network. To better understand the effect of the ionic strength on the nanostructure of the material, non-invasive and high-resolution imaging techniques, such as X-ray nanotomography, should be employed. This was, however, beyond the scope of this investigation.

The dry and wet mechanical properties of the aerogels were evaluated using a single compression cycle and a maximum strain of 80%. Compression curves of porous materials generally show three distinct regions: a low-strain region where the cell wall displays elastic stretching and bending, an intermediate-strain region where the cell walls collapse and a high-strain region where the material densifies as opposite cell walls come in contact with each other.[63] As shown in Figure 3d, aerogels prepared from CNF gels of higher solid contents are mechanically stronger in the dry state, both in the intermediate and in the high strain regions. This indicates that a larger mechanical stress in needed to collapse and compress cell walls of higher densities. As displayed in Figure S1 (Supporting Information), increasing the solid content of the CNF gel (from 7.5 to 19.5 g L^{-1}) also resulted in aerogels with higher density (from 24 to 39 kg m^{-3}) and compressive stiffness (from 97 to 275 kPa), which is in good accordance with previously reported work.[36,64] In the elastic deformation regime, the aerogels benefit from the outstanding stiffness of the CNFs, thus explaining their high elastic moduli to density ratios. As shown in Figure S2 (Supporting Information), aerogels present similar compressive behaviors when prepared with ionic strength additions of 10 and 100×10^{-3} M. Consequently, the dry-state mechanical properties of the aerogels mainly rely on the solid content of the CNF gel.

As discussed, the preparation of aerogels that are mechanically strong in the wet state relies on the inclusion of alginate. Figure 3e shows the compression behavior of wet aerogels presenting two different CNF-to-alginate ratios (50:50 and 80:20). Prior to testing, the samples were soaked from the dry state in a 1 M $CaCl_2$, thus made wet-stable. The 50:50 samples are stronger than the 80:20 in the densification regime, while no obvious difference can be seen in the initial stages of compression. Therefore, this strength enhancement is a plausible consequence of an increase in density (from 39 ± 3 kg m^{-3} for the 80:20 samples to 55 ± 5 kg m^{-3} for the 50:50 samples), and not due to a better wet-stabilization of the structure.

2.4. Material Shaping Considerations: Toward 3D Printing

Advanced technological applications require materials that are easily prepared into a large array of shapes. For instance, the design of many electronic devices often involves materials with complex shapes, formed with a submillimeter resolution. This holds even more true for medical applications, such as tissue engineering and wound healing, where the materials have to be geometrically tailored with high precision.

In this respect, 3D printing enables a fast and continuous preparation of products of virtually any shape. Gel-like materials are readily printed using pressure-driven printers, also known as bioprinters. Alginate and CNF mixtures have already been demonstrated as being suitable for 3D printing,[44,65,66] as the ratio of alginate to CNF and the ionic strength give a precise control over the viscosity of the gel, making it possible to print thin and stable gel layers. As shown in **Figure 4**, a 3D-printing step can be implemented in the aerogel preparation route. Alginate and CNF mixtures can be printed into intricate shapes and successively frozen, thawed, solvent exchanged, and dried into highly porous networks. Figure 4b–d shows aerogels made by 3D-printing of 80:20 10×10^{-3} M $CaCl_2$ gels. Figure 4b shows an aerogel shaped as a honeycomb; before and after drying with acetone. Although a shrinkage was observed upon drying, the structural features were preserved and the resulting aerogel shows a submillimeter patterning resolution. Figure 4c,d

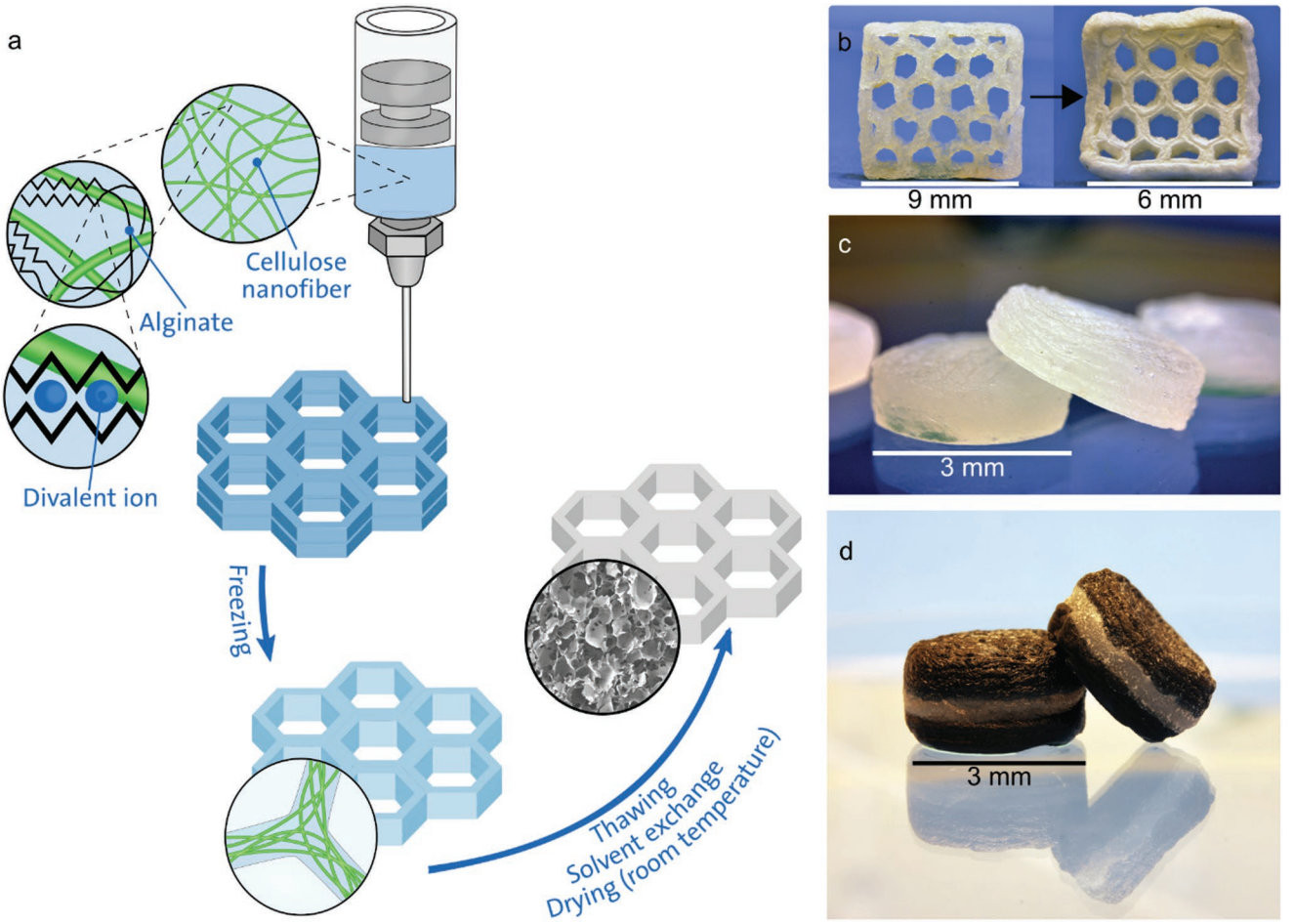

Figure 4. a) Schematic summary of the protocol for the 3D printing of alginate and CNFs mixtures and subsequent aerogel fabrication. Photos of b) 3D-printed aerogel grids before (left) and after (right) drying, c) 3D-printed aerogels of cylindrical shape, and d) layered aerogels that were 3D-printed by a dual-extrusion approach where the dark layers contain a mixture of CNFs, alginate, and PEDOT:PSS, and the translucent layer a mixture of CNFs and alginate (the samples shown on (c) and (d) have been soaked in water).

show cylindrical aerogels prepared by 3D printing eight layers of material, using a simple and dual extrusion approach, respectively. For the latter, two different printing heads were used to achieve the layered structure shown in Figure 4d: one containing a mixture of CNFs, alginate and poly(3,4-ethylenedioxythiophene) polystyrene sulfonate (PEDOT:PSS) (dark layers) and one containing a mixture of CNFs and alginate (translucent layers). No visible diffusion of the PEDOT:PSS from the dark to the translucent layers was observed throughout the preparation of layered aerogels. This observation was further confirmed by connecting an ohmmeter to the two PEDOT rich regions, showing the absence of an electrically conducting path through the separating layer. This demonstrates the possibility of preparing aerogel supercapacitors through additive manufacturing, where the two PEDOT:PSS-containing sections act as electrodes, separated by insulating layers containing CNFs and alginate. The use of aerogels for energy storage applications is further discussed in Section 3.2.

3. PEDOT:TOS-Functionalized Aerogels

3.1. An In Situ Polymerization Approach

PEDOT is commercially available as aqueous dispersions of PEDOT:PSS colloidal complexes, which have been extensively used together with CNFs to prepare conducting composites.[53,67,68] These dispersions are, however, only available in low concentrations, typically between 1.3 and 5 wt%, thus making the preparation of materials with high PEDOT loadings rather tedious. Moreover, a significant excess of non-conducting PSS is used in these formulations to increase the dispersibility of the colloidal complexes in water. Large volumes of organic solvents, such as DMSO or ethylene glycol, are then required to remove this surplus and create a conducting pathway in the PEDOT:PSS treated materials. Alternatively, high PEDOT loading can be achieved by polymerizing 3,4-ethylenedioxythiophene (EDOT). The post-treatment in organic solvents can be circumvented by using a smaller counterion, such as tosylate (TOS), instead of PSS. PEDOT polymerization is typically done by either vapor phase polymerization or aqueous-oxidative polymerization.[52] These polymerization approaches can be used to functionalize surfaces provided there is good chemical affinity with PEDOT. Han et al. have reported an aqueous synthesis of PEDOT nanoparticles using EDOT, p-Toluenesulfonic acid (PTSA) as dopant and ammonium persulfate (APS) as initiator of the polymerization.[69] When using a methanolic silica solution as the reaction media, they demonstrated the successful polymerization of EDOT onto the surface of the nanosilica network.[70]

A similar polymerization procedure was used to functionalize the prepared aerogels (see Experimental Section), shown in **Figure 5**a, yielding EDOT conversion rates of typically 25–47% (see Supporting Information for the calculations).

Figure 5b,c show the microstructure of an 80:20 10×10^{-3} M $CaCl_2$ aerogel functionalized with PEDOT:TOS, at a material loading of 1.7 g g^{-1} (mass of PEDOT:TOS per gram of aerogel). These micrographs show that the internal surfaces of the aerogels are completely covered with spherical nanoparticles

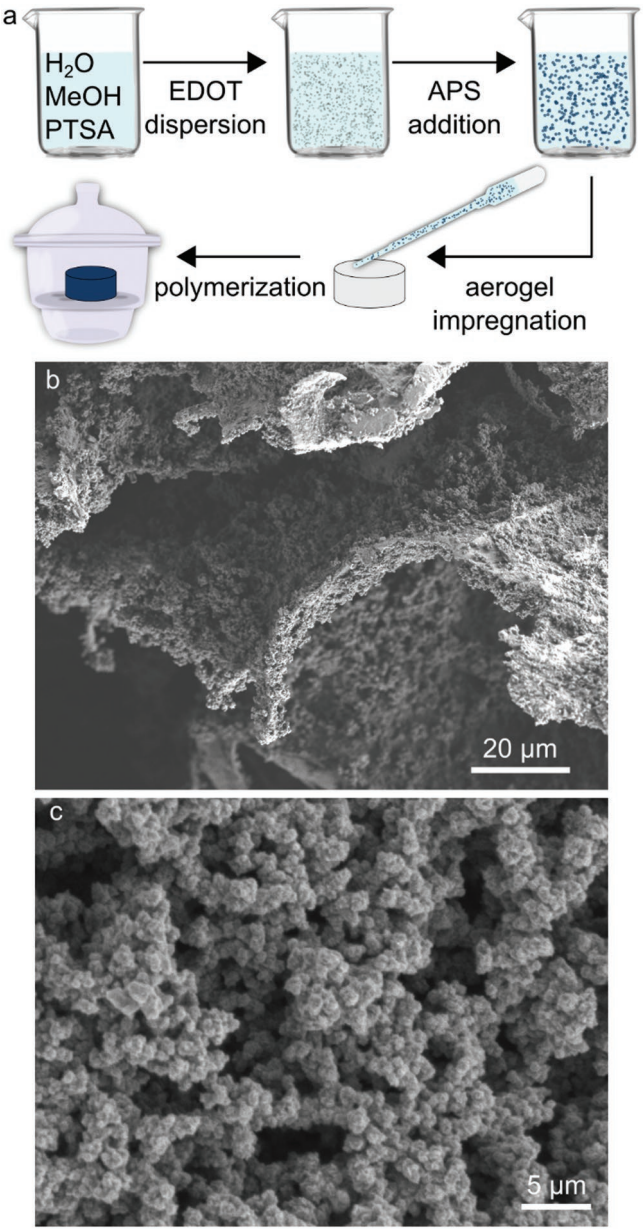

Figure 5. a) Schematic of the experimental procedure used for the in situ polymerization of EDOT in aerogels. b) SEM micrograph of an internal surface of a PEDOT:TOS-functionalized aerogel and c) magnification of the surface shown in (b), showing how the PEDOT:TOS nanoparticles cover one of the inner surfaces of the aerogel.

of PEDOT:TOS. Due to the hydrophobic nature of both the EDOT and PEDOT:TOS, the nanoparticles precipitate on the surfaces of the aerogel. Different PEDOT loadings can be achieved by changing the EDOT concentration in the reaction mixture (while adjusting the APS and PTSA concentrations accordingly). The samples showed an electrical conductivity as high as 5.7 S m^{-1}, measured using a 4-point probe. In order to compare the electrical properties of materials of different densities, the reported conductivities are generally normalized by the volume fraction occupied by the conducting component

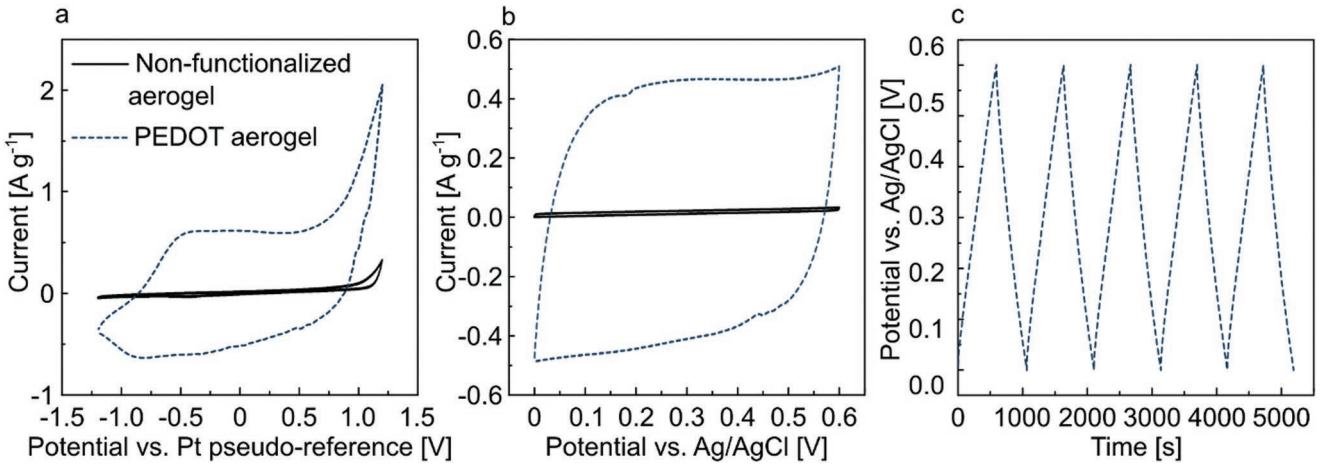

Figure 6. Voltammograms of a PEDOT-functionalized aerogel and a non-functionalized aerogel at a sweep rate of 5 mV s^{-1}; measured in a) acetonitrile with 0.1 M TBAHFP and b) water with 0.1 M NaCl. c) Galvanostatic charge–discharge profile of a PEDOT-functionalized aerogel at a current of 0.1 A g^{-1}.

(see Supporting Information). The normalized conductivity of the PEDOT-functionalized aerogels was calculated to be 146 ± 8 S m^{-1}. This value compares well with the one reported in recently published studies regarding aerogels solely made from freeze-dried PEDOT:PSS dispersions.[71–73] This result is remarkable since the cellulose and alginate represent a large weight fraction of the material (37% at a loading of 1.7 g g^{-1}), and can be considered as electrical insulators. No substantial variation in the electrical conductivity was found when comparing PEDOT loadings of 1 and 1.7 g g^{-1}, as a fully interconnected network of PEDOT nanoparticles was already observed at loadings of 1 g g^{-1}.

3.2. Application as Energy Storage Materials

Figure 6a shows a typical cyclic voltammogram (CV) obtained from PEDOT-functionalized aerogels, compared to a non-functionalized aerogel (see Supporting Information for more details about this experimental procedure). These measurements were carried out in acetonitrile using 0.1 M tetrabutylammonium hexafluorophosphate (TBAHFP), enabling a scan of a larger voltage window than possible in water. The shape of the CV curve is similar to those reported in previous studies, showing a large supercapacitive region (between –0.6 and 0.6 V vs. a Pt pseudo-reference electrode) and irreversible PEDOT oxidation at high positive potentials.[74]

The results shown in Figure 6b,c were obtained from measurements in water using 0.1 M NaCl as supporting electrolyte. Supercapacitive behavior is observed in the 0–0.6 V region, using low voltage-sweep rates and charge/discharge currents, indicated by the square shape of the CV curve shown in Figure 6b, as well as the absence of a significant voltage drop during cycling (Figure 6c). As shown in Table S1 (Supporting Information), the measured specific capacitance, i.e., capacitance normalized with the mass of active substance, was as high as 78 F g^{-1} at 0.1 A g^{-1} (or 49 F g^{-1}, when instead normalized with the total mass, including CNF and alginate), which is in good accordance with previous investigations.[75,76]

3.3. Application as Pressure and Humidity Sensors

Conducting aerogels have historically been used in numerous sensing applications as their electrical conductivity is generally sensitive to external stresses. Depending on the structure and chemical nature of the aerogels, they can be used to measure physical quantities such as temperature, mechanical stress, humidity, and the presence of specific gases.[68,77–79]

When compressed in the wet-state, the PEDOT-functionalized aerogels show an increase in electrical conductivity, as the bending and densification of the cell walls lead to the formation of more contacts between the PEDOT-rich regions. If the mechanical deformation is reversible, the stress or strain levels of such aerogels could be determined by measuring their electrical conductivity. As shown in **Figure 7**a, the use of PEDOT-functionalized aerogels as pressure sensors was studied by measuring the material's resistance upon cyclic compressive deformation. During compression, the resistance slowly decreases in the cell-wall bending region before drastically decreasing at the onset of densification (when opposite PEDOT-covered surfaces are compacted together). Consequently, the resistance of the material does not scale linearly with the compression and seems to follow its different regimes of deformation. During the first compressive cycle, the resistance of the material decreased from 20 Ω to 10 Ω during loading before increasing up to almost 60 Ω upon unloading. The observed increase in resistance in the unloaded state (from 20 Ω to 60 Ω) is most-likely due to mechanical damage inflicted to the PEDOT structure during the first cycle. However, on repeated compression–decompression cycles, the resistance would reversibly cycle between 10 Ω (compressed) and 60 Ω (decompressed), thus demonstrating the sought-after, pressure sensor behavior (see Supporting Information for a mathematical fitting of a compression/decompression cycle).

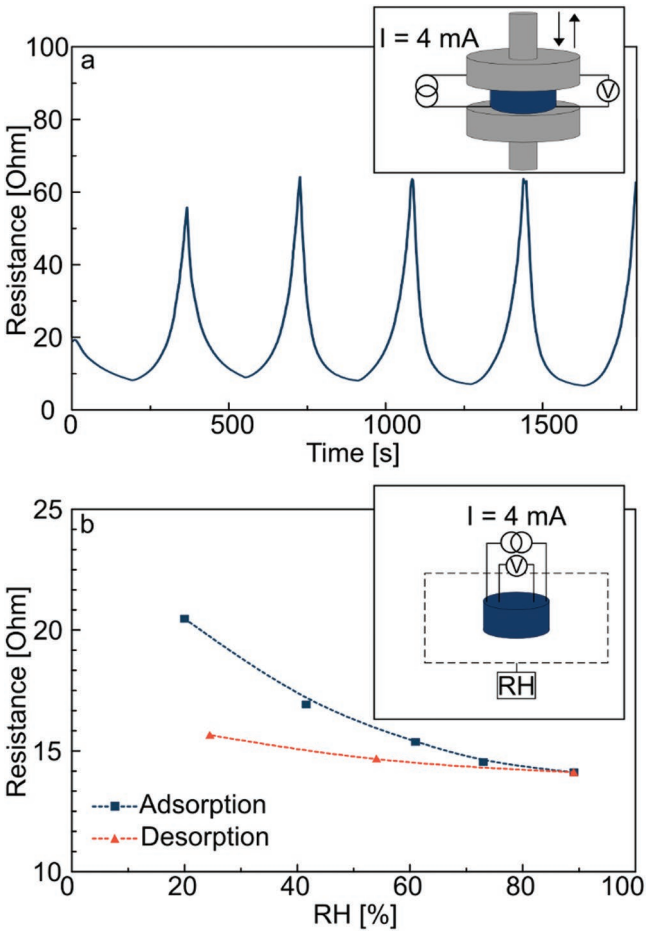

Figure 7. a) Resistance of a PEDOT-functionalized aerogel during five consecutive cycles of compression. b) Resistance of a PEDOT-functionalized aerogel as a function of the surrounding relative humidity.

As cellulose is a hygroscopic material that changes dimension as it sorbs water, it has also been used to design moisture sensors.[80] Therefore, the PEDOT-functionalized aerogels were tested for humidity sensing. Figure 7b shows that the material's resistance gradually decreases from 20 Ω at 20% RH to 15 Ω at 90% RH. This result is noteworthy, as the electrical performance of PEDOT-based materials is generally degraded in humid conditions.[52] As the humidity increases, more water sorbs in the cellulose structure, causing it to swell and, presumably, increasing the contact area between the PEDOT-covered surfaces. When the humidity later is decreased, water is desorbed, the structure shrinks and the material becomes less conducting. The plot shown in Figure 7b, however, presents a rather large hysteresis. This is not surprising since each humidity step of this experiment was only maintained over 30 min and it usually requires longer times for cellulose to reach its equilibrium moisture content (especially during desorption, which is a slower process). Furthermore, cellulose is known to display sorption hysteresis even at equilibrium conditions, but a recent study shows that the hysteresis can be removed by using modified grades of cellulose;[81] therefore, it is presumably feasible to prepare sensors where the relative humidity is a true function of the electrical conductivity of the aerogel.

4. Conclusion

A novel, green, and efficient way of preparing wet-stable aerogels from CNFs and alginate has been demonstrated. Relying on simple freezing, solvent exchange and ambient drying steps, this method could enable a large-scale production of cellulosic aerogels, which has hitherto been unachievable.

It has also been shown that the ionic strength in the CNF gel governs the structure and mechanical properties of the aerogels. By using a controlled addition of salt, in this case NaCl or $CaCl_2$, the volumetric shrinkage of the aerogels during drying was reduced to 30% (as opposed to a complete collapse). When preparing aerogels from CNF gels of different solid contents, their mechanical properties in the dry state were shown to scale with an increase in their density; with elastic moduli as high as 275 kPa at a density of 39 kg m^{-3}.

The aerogels were successfully made wet-stable when soaked in concentrated calcium solutions, making them suitable for use in applications where wet integrity is a pre-requisite; such as cell-growth scaffolds and organic electronics. This novel post-treatment method is simpler and greener than the current state-of-the-art crosslinking methods and makes the process suitable for industrial scale manufacturing of wet-stable aerogels. In combination with this, the ability to 3D print the aerogels has also been demonstrated which allows the mass production of aerogels in any printable shape, a distinct advantage for some applications such as tissue engineering where each device needs to be individually shaped with high precision.

Finally, to demonstrate the usefulness of these aerogels in the field of organic electronics, we developed an aqueous in situ polymerization protocol to functionalize the material with PEDOT. Electrical conductivities of 146 S m^{-1} were achieved with loadings of 1.7 g of PEDOT:TOS per gram of aerogel. These functionalized aerogels were shown to be particularly interesting as energy storage materials, showing specific capacitances as high as 78 F g^{-1}. Additionally, their use as mechanical deformation and relative humidity sensors has been demonstrated.

5. Experimental Section

Materials: CNFs (carboxymethylated with a total charge of 600 ± 50 µmol g^{-1}) were provided by RISE Bioeconomy AB in the form of a 2 wt% aqueous gel (see Supporting Information for a complete description of the preparation procedure). Sodium alginate (high viscosity) was purchased from VWR International. PEDOT:PSS (CLEVIOS™ PH 1000) was purchased from Heraeus. NaCl (≥99.0%), $CaCl_2$ (dihydrate, ≥99.0%), PTSA (monohydrate, ≥98.5%), APS (≥98.0%), TBAHFP (≥99.0%), and acetonitrile (anhydrous, ≥99.8%) were purchased from Sigma Aldrich. EDOT (97%) was purchased from Alfa Aesar.

Aerogel Preparation Procedure: CNFs, alginate, and salt (from concentrated solutions of sodium chloride or calcium chloride) were mixed together using a using a high-shear mixer (Ultra-Turrax T25®, Ika), in batches of 100 g, at 14 000 rpm. All samples, apart from the ones displayed in Figure 3c, were prepared using a CNF solid content of 19.5 g L^{-1}. The gel mixtures were then cast into closed cylindrical polystyrene molds, frozen at −18 °C and kept at this temperature overnight to ensure a complete freezing. The samples were then thawed by submerging the molds in ethanol. Once completely thawed, the samples were removed from the molds, solvent exchanged to acetone

by a total of three, 30 min long, consecutive steps and, finally, allowed to dry under ambient conditions.

3D Printing: The 3D printing of CNF and alginate gels was carried out using a BIO X 3D bioprinter (Cellink®). The bioprinter uses piston-driven syringe heads and the material flow is regulated by the print pressure. Great attention was paid not to introduce air bubbles while mixing the gel and transferring it to the syringe heads. The gels were printed at room temperature using 410 µm high-precision conical nozzles at a print pressure of 20–40 kPa. Since gels of different formulations present large disparities in viscosity, the print head speed and print pressure were manually adjusted for each print.

In Situ Polymerization of PEDOT:TOS: EDOT (0.2 g L^{-1}) was vigorously dispersed in an aqueous solution of methanol (2 vol%) and PTSA (1 M). The polymerization was triggered by the addition of APS in equimolar ratio with EDOT. The mixture was then quickly stirred, poured onto, and absorbed into the aerogel before being left to polymerize for 24 h. Cylindrical aerogels with a diameter, height, and weight of approximatively 30 mm, 9 mm, and 250 mg, respectively were fully saturated with 5.5 mL of solution. The solutions were typically prepared in 20 mL vials. The mixing steps were carried out using a vortex mixer (VWR International). In order to prevent evaporation of the water-methanol solution, the aerogel was placed into a desiccator previously saturated with water vapor. The aerogel was thereafter soaked in large volumes of Milli-Q water to remove the APS and excess PTSA and then in ethanol to rinse away any remaining unreacted EDOT. Prior to ambient drying, the functionalized aerogels were solvent-exchanged to acetone. The polymerization and rinsing steps were both carried out at room temperature.

Supporting Information

Supporting Information is available from the Wiley Online Library or from the author.

Acknowledgements

This work was supported by the Swedish Stiftelsen för Strategisk Forskning (SSF) through the 0D + 1D + 2D = 3D project. The authors also acknowledge the support of the 3D Bioprinting Center (Chalmers University of Technology, Gothenburg, Sweden), the Division of Wood Chemistry and Pulp Technology (Prof. Monika Ek, KTH Royal Institute of Technology, Stockholm, Sweden), the Wenner-Gren Foundation, the Swedish Research Council Formas, Nouryon AB, and the Wallenberg Wood Science Center.

Conflict of Interest

The authors declare no conflict of interest.

Keywords

aerogels, cellulose, nanofibers, organic electronics, poly(3,4-ethylenedioxythiophene)

Received: November 10, 2019
Revised: December 18, 2019
Published online: February 3, 2020

[1] S. S. Kistler, *Nature* **1931**, *127*, 741.
[2] J. Fricke, *J. Non-Cryst. Solids* **1988**, *100*, 169.
[3] L. W. Hrubesh, *J. Non-Cryst. Solids* **1998**, *225*, 335.
[4] A. D. McNaught, A. Wilkinson, *IUPAC Compendium of Chemical Terminology*, Blackwell Science, Hoboken, NJ **1997**.
[5] M. A. Aegerter, N. Leventis, M. M. Koebel, *Aerogels Handbook*, Springer, London, United Kingdom **2011**.
[6] M. Schmidt, F. Schwertfeger, *J. Non-Cryst. Solids* **1998**, *225*, 364.
[7] D. M. Smith, A. Maskara, U. Boes, *J. Non-Cryst. Solids* **1998**, *225*, 254.
[8] M. S. Ahmed, Y. A. Attia, *J. Non-Cryst. Solids* **1995**, *186*, 402.
[9] P. Xu, J. E. Drewes, D. Heil, G. Wang, *Water Res.* **2008**, *42*, 2605.
[10] A. E. Fischer, M. P. Saunders, J. C. Lytle, D. R. Rolison, J. W. Long, *ECS Trans.* **2008**, *6*, 159.
[11] E. Baudrin, G. Sudant, D. Larcher, B. Dunn, J. M. Tarascon, *Chem. Mater.* **2006**, *18*, 4369.
[12] H. Im, T. Kim, H. Song, J. Choi, J. S. Park, R. Ovalle-Robles, H. D. Yang, K. D. Kihm, R. H. Baughman, H. H. Lee, T. J. Kang, Y. H. Kim, *Nat. Commun.* **2016**, *7*, 10600.
[13] M. O. Adebajo, R. L. Frost, J. T. Kloprogge, O. Carmody, S. Kokot, *J. Porous Mater.* **2003**, *10*, 159.
[14] V. Gibiat, O. Lefeuvre, T. Woignier, J. Pelous, J. Phalippou, *J. Non-Cryst. Solids* **1995**, *186*, 244.
[15] a) N. Hüsing, U. Schubert, *Angew. Chem., Int. Ed.* **1998**, *37*, 22; b) N. Hüsing, U. Schubert, *Angew. Chem.* **1998**, *110*, 22.
[16] D. M. Smith, D. Stein, J. M. Anderson, W. Ackerman, *J. Non-Cryst. Solids* **1995**, *186*, 104.
[17] G. Herrmann, R. Iden, M. Mielke, F. Teich, B. Ziegler, *J. Non-Cryst. Solids* **1995**, *186*, 380.
[18] K. E. Parmenter, F. Milstein, *J. Non-Cryst. Solids* **1998**, *223*, 179.
[19] G. Carlson, D. Lewis, K. McKinley, J. Richardson, T. Tillotson, *J. Non-Cryst. Solids* **1995**, *186*, 372.
[20] R. W. Pekala, J. C. Farmer, C. T. Alviso, T. D. Tran, S. T. Mayer, J. M. Miller, B. Dunn, *J. Non-Cryst. Solids* **1998**, *225*, 74.
[21] A. E. Aliev, J. Oh, M. E. Kozlov, A. A. Kuznetsov, S. Fang, A. F. Fonseca, R. Ovalle, M. D. Lima, M. H. Haque, Y. N. Gartstein, M. Zhang, A. A. Zakhidov, R. H. Baughman, *Science* **2009**, *323*, 1575.
[22] F. Tanaka, T. Iwata, *Cellulose* **2006**, *13*, 509.
[23] T. Nishino, K. Takano, K. Nakamae, *J. Polym. Sci., Part B: Polym. Phys.* **1995**, *33*, 1647.
[24] a) D. Klemm, F. Kramer, S. Moritz, T. Lindström, M. Ankerfors, D. Gray, A. Dorris, *Angew. Chem., Int. Ed.* **2011**, *50*, 5438; b) D. Klemm, F. Kramer, S. Moritz, T. Lindström, M. Ankerfors, D. Gray, A. Dorris, *Angew. Chem.* **2011**, *123*, 5550.
[25] T. Saito, S. Kimura, Y. Nishiyama, A. Isogai, *Biomacromolecules* **2007**, *8*, 2485.
[26] T. Saito, Y. Nishiyama, J. L. Putaux, M. Vignon, A. Isogai, *Biomacromolecules* **2006**, *7*, 1687.
[27] A. Isogai, T. Saito, H. Fukuzumi, *Nanoscale* **2011**, *3*, 71.
[28] L. Wågberg, G. Decher, M. Norgren, T. Lindström, M. Ankerfors, K. Axnäs, *Langmuir* **2008**, *24*, 784.
[29] A. B. Fall, S. B. Lindström, O. Sundman, L. Ödberg, L. Wågberg, *Langmuir* **2011**, *27*, 11332.
[30] A. B. Fall, S. B. Lindström, J. Sprakel, L. Wågberg, *Soft Matter* **2013**, *9*, 1852.
[31] N. Lavoine, L. Bergström, *J. Mater. Chem. A* **2017**, *5*, 16105.
[32] K. J. De France, T. Hoare, E. D. Cranston, *Chem. Mater.* **2017**, *29*, 4609.
[33] N. T. Cervin, C. Aulin, P. T. Larsson, L. Wågberg, *Cellulose* **2012**, *19*, 401.
[34] J. T. Korhonen, M. Kettunen, R. H. A. Ras, O. Ikkala, *ACS Appl. Mater. Interfaces* **2011**, *3*, 1813.
[35] G. Nyström, A. Marais, E. Karabulut, L. Wågberg, Y. Cui, M. M. Hamedi, *Nat. Commun.* **2015**, *6*, 7259.
[36] J. Erlandsson, V. López Durán, H. Granberg, M. Sandberg, P. A. Larsson, L. Wågberg, *Appl. Mater. Today* **2016**, *5*, 246.

[37] H. Liu, A. Wang, X. Xu, M. Wang, S. Shang, S. Liu, J. Song, *RSC Adv.* **2016**, *6*, 42854.
[38] a) M. Hamedi, E. Karabulut, A. Marais, A. Herland, G. Nyström, *Angew. Chem., Int. Ed.* **2013**, *52*, 12038; b) M. Hamedi, E. Karabulut, A. Marais, A. Herland, G. Nyström, L. Wågberg, *Angew. Chem.* **2013**, *125*, 12260.
[39] J. Erlandsson, H. Françon, A. Marais, H. Granberg, L. Wågberg, *Biomacromolecules* **2019**, *20*, 728.
[40] S. H. Zeronian, F. L. Hudson, R. H. Peters, *Tappi* **1964**, *47*, 557.
[41] J. Erlandsson, T. Pettersson, T. Ingverud, H. Granberg, P. A. Larsson, M. Malkoch, L. Wågberg, *J. Mater. Chem. A* **2018**, *6*, 19371.
[42] S. Koprivica, M. Siller, T. Hosoya, W. Roggenstein, T. Rosenau, A. Potthast, *ChemSusChem* **2016**, *9*, 825.
[43] H. Liimatainen, J. Sirviö, H. Pajari, O. Hormi, J. Niinimäki, *J. Wood Chem. Technol.* **2013**, *33*, 258.
[44] K. Markstedt, A. Mantas, I. Tournier, H. Martínez Ávila, D. Hägg, P. Gatenholm, *Biomacromolecules* **2015**, *16*, 1489.
[45] P. Krontiras, P. Gatenholm, D. A. Hagg, *J. Biomed. Mater. Res., Part B* **2015**, *103*, 195.
[46] T. Benselfelt, J. Engström, L. Wågberg, *Green Chem.* **2018**, *20*, 2558.
[47] H. Andriamanantoanina, M. Rinaudo, *Polym. Int.* **2010**, *59*, 1531.
[48] L. Li, Y. Fang, R. Vreeker, I. Appelqvist, E. Mendes, *Biomacromolecules* **2007**, *8*, 464.
[49] G. T. Grant, E. R. Morris, D. A. Rees, P. J. C. Smith, D. Thom, *FEBS Lett.* **1973**, *32*, 195.
[50] G. Nyström, A. Mihranyan, A. Razaq, T. Lindström, L. Nyholm, M. Strømme, *J. Phys. Chem. B* **2010**, *114*, 4178.
[51] C. Long, D. Qi, T. Wei, J. Yan, L. Jiang, Z. Fan, *Adv. Funct. Mater.* **2014**, *24*, 3953.
[52] A. Elschner, S. Kirchmeyer, W. Lövenich, U. Merker, K. Reuter, *PEDOT: Principles and Applications of an Intrinsically Conductive Polymer*, CRC Press, Boca Raton, FL **2010**.
[53] A. Malti, J. Edberg, H. Granberg, Z. U. Khan, J. W. Andreasen, X. Liu, D. Zhao, H. Zhang, Y. Yao, J. W. Brill, I. Engquist, M. Fahlman, L. Wågberg, X. Crispin, M. Berggren, *Adv. Sci.* **2016**, *3*, 1500305.
[54] J. Edberg, A. Malti, H. Granberg, M. M. Hamedi, X. Crispin, I. Engquist, M. Berggren, *Flexible Printed Electron.* **2017**, *2*, 045010.
[55] D. Belaineh, J. W. Andreasen, J. Palisaitis, A. Malti, K. Håkansson, L. Wågberg, X. Crispin, I. Engquist, M. Berggren, *ACS Appl. Polym. Mater.* **2019**.
[56] A. Y. Mehandzhiyski, I. Zozoulenko, *ACS Appl. Energy Mater.* **2019**, *2*, 3568.
[57] S. Deville, *J. Mater. Res.* **2013**, *28*, 2202.
[58] T. Benselfelt, M. Nordenström, M. M. Hamedi, L. Wågberg, *Nanoscale* **2019**, *11*, 3514.
[59] F. Martoïa, T. Cochereau, P. J. J. Dumont, L. Orgéas, M. Terrien, M. N. Belgacem, *Mater. Des.* **2016**, *104*, 376.
[60] B. Miller, I. Tyomkin, *J. Colloid Interface Sci.* **1994**, *162*, 163.
[61] W. B. Bald, in *Food Freezing: Today and Tomorrow*, 1st edition (Ed: W. B. Bald), Springer, London, United Kingdom, **1991**, Ch. 5.
[62] P. K. Chatterjee, B. S. Gupta, in *Textile Science and Technology*, Vol. *13*, (Eds: P. K. Chatterjee, B. S. Gupta), Elsevier, Amsterdam, Netherlands, **2002**, Ch. 1.
[63] M. R. Ashby, R. Medalist, *Metall. Soc. AIME* **1983**, *14*, 1755.
[64] H. Sehaqui, Q. Zhou, L. A. Berglund, *Compos. Sci. Technol.* **2011**, *71*, 1593.
[65] D. Nguyen, D. Hägg, A. Forsman, J. Ekholm, P. Nimkingratana, C. Brantsing, T. Kalogeropoulos, S. Zaunz, S. Concaro, M. Brittberg, A. Lindahl, P. Gatenholm, A. Enejder, S. Simonsson, *Sci. Rep.* **2017**, *7*, 658.
[66] V. C. F. Li, A. Mulyadi, C. K. Dunn, Y. Deng, H. J. Qi, *ACS Sustainable Chem. Eng.* **2018**, *6*, 2011.
[67] Z. U. Khan, J. Edberg, M. M. Hamedi, R. Gabrielsson, H. Granberg, L. Wågberg, I. Engquist, M. Berggren, X. Crispin, *Adv. Mater.* **2016**, *28*, 4556.
[68] S. Han, F. Jiao, Z. U. Khan, J. Edberg, S. Fabiano, X. Crispin, *Adv. Funct. Mater.* **2017**, *27*, 1703549.
[69] M. G. Han, S. H. Foulger, *Chem. Commun.* **2004**, *10*, 2154.
[70] M. G. Han, S. P. Armes, *Langmuir* **2003**, *19*, 4523.
[71] G. Chen, R. Rastak, Y. Wang, H. Yan, V. Feig, Y. Liu, Y. Jiang, S. Chen, F. Lian, F. Molina-Lopez, L. Jin, K. Cui, J. W. Chung, E. Pop, C. Linder, Z. Bao, *Matter* **2019**, *1*, 205.
[72] X. Zhang, C. Li, Y. Luo, *Langmuir* **2011**, *27*, 1915.
[73] A. G. Guex, J. L. Puetzer, A. Armgarth, E. Littmann, E. Stavrinidou, E. P. Giannelis, G. G. Malliaras, M. M. Stevens, *Acta Biomater.* **2017**, *62*, 91.
[74] M. Bongo, O. Winther-Jensen, S. Himmelberger, X. Strakosas, M. Ramuz, A. Hama, E. Stavrinidou, G. G. Malliaras, A. Salleo, B. Winther-Jensen, R. M. Owens, *J. Mater. Chem. B* **2013**, *1*, 3860.
[75] K. Lota, V. Khomenko, E. Frackowiak, *J. Phys. Chem. Solids* **2004**, *65*, 295.
[76] K. Wijeratne, M. Vagin, R. Brooke, X. Crispin, *J. Mater. Chem. A* **2017**, *5*, 19619.
[77] H. Qi, J. Liu, J. Pionteck, P. Pötschke, E. Mäder, *Sens. Actuators, B.* **2015**, *213*, 20.
[78] M. Wang, I. V. Anoshkin, A. G. Nasibulin, J. T. Korhonen, J. Seitsonen, J. Pere, E. I. Kauppinen, R. H. A. Ras, O. Ikkala, *Adv. Mater.* **2013**, *25*, 2428.
[79] S. Han, N. U. H. Alvi, L. Granlöf, H. Granberg, M. Berggren, S. Fabiano, X. Crispin, *Adv. Sci.* **2019**, *6*, 1802128.
[80] a) F. Güder, A. Ainla, J. Redston, B. Mosadegh, A. Glavan, T. J. Martin, G. Whitesides, *Angew. Chem., Int. Ed.* **2016**, *55*, 5727; b) F. Güder, A. Ainla, J. Redston, B. Mosadegh, A. Glavan, T. J. Martin, G. Whitesides, *Angew. Chem.* **2016**, *128*, 5821.
[81] P. A. Larsson, M. Gimåker, L. Wågberg, *Cellulose* **2008**, *15*, 837.